Grant Agreement No.: 604656

Project acronym: NanoSim

Project title: A Multiscale Simulation-Based Design Platform for Cost-Effective CO_2 Capture Processes using Nano-Structured Materials (NanoSim)

Funding scheme: Collaborative Project

Thematic Priority: NMP

THEME: [NMP.2013.1.4-1] Development of an integrated multi-scale modelling environment for nanomaterials and systems by design

Starting date of project: 1st of January, 2014

Duration: 48 months

WP N°	Del. N°	Title	Contributors	Version	Lead beneficiary	Nature	Dissemin. level	Delivery date from Annex I	Actual delivery date dd/mm/yyyy
3	3.3	Defect formation energies and dynamic stability of metal/metal-oxide nanoparticle with support determined	Stephen Shevlin	1	3	R	PU	31/12/2015	24/06/2016

Introduction

In this Deliverable we compare the structural and thermodynamic properties of several prospective barrier materials for the oxygen carrying (OC) material haematite Fe_2O_3. We discuss the stability of these materials with respect to temperature, and Fe inclusion, and determine their suitability as barriers for separating the oxygen carrier from the alumina Al_2O_3 support. This is essential as, without this barrier material, the haematite and the alumina can react at high temperature to form intermediate compounds that are inactive for Chemical Looping Reforming, such as Al_2FeO_4 or $AlFeO_3$, see Figure 1. This results in loss of active material, effecting the efficiency of the plant.

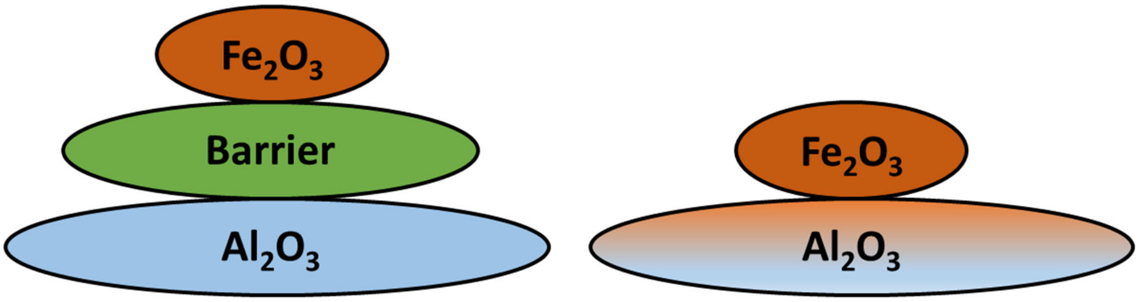

Figure 1: Design of active material support. On the left-hand side the active material is physically separated from the thermal support by the barrier material. On the right-hand side this is not the case, resulting in leaching of Fe into the support.

Based on directions from D_3.1 and from our experimental colleagues in Norway, specifically Dr Anita Fossdal, we focussed attention on barium hexaaluminate (BAHO) and related materials such as strontium or calcium hexaaluminate (CAH[1]O). As discussed in that document, these materials are the only ones in the literature that have being reported to stabilize OC materials.

Methodology

We used Density Functional Theory to determine the thermodynamics and structural properties of several hexaaluminates.[2] A plane wave cutoff of 450 eV was used, while a Monkhorst-Pack net of (2×2×2) k-points was used to sample the Brillouin zone. In order to minimize the dopant interactions between periodic images, a (2×2×1) supercell was used. The *c*-axis for both materials studied was considerably longer than the *a*- and *b*- axes, therefore in order to reduce computational time there was no doubling along this axis. We also modelled the bulk cell of Haematite for comparison of lattice expansion properties. In order to properly model the localisation of the Fe *d*-states we used the GGA+U formalism, as implemented with the Dudarev algorithm.[3] Here, we used an effective *U* value of 4.2 eV, a similar value to others in the literature.[4]

Crystal structure

We model both BAHO and CAHO crystal structures. BAHO was suggested as a candidate support material from D_3.1, however as pointed out in that document the presence of barium may result in issues with toxicity, therefore it would be preferable to replace this element with a safer alternative.

CAHO, where the barium is replaced with safer calcium, has an extremely similar crystal structure. This material was also investigated.

The chemical formula of BAHO and CAHO is $BaO·(Al_2O_3)_6$ and $CaO·(Al_2O_3)_6$ respectively, with barium and calcium atoms oxidation state 2^+, oxygen atoms 2^-, and aluminium atoms 3^+. A large proportion of the experimental crystal structure of BAHO is defective, for example containing multiple Al and O vacancies. It is a requirement for crystal stability that ionic charge is balanced. Our initial work thus focussed on the properties of a $BaAl_{11}O_{17.5}$ supercell based on experimental data. However, from analysis of the DOS (Density of States), we observe that there are plenty of gap defect states, see Figure 2. This would complicate any thermodynamic analysis for Fe incorporation.

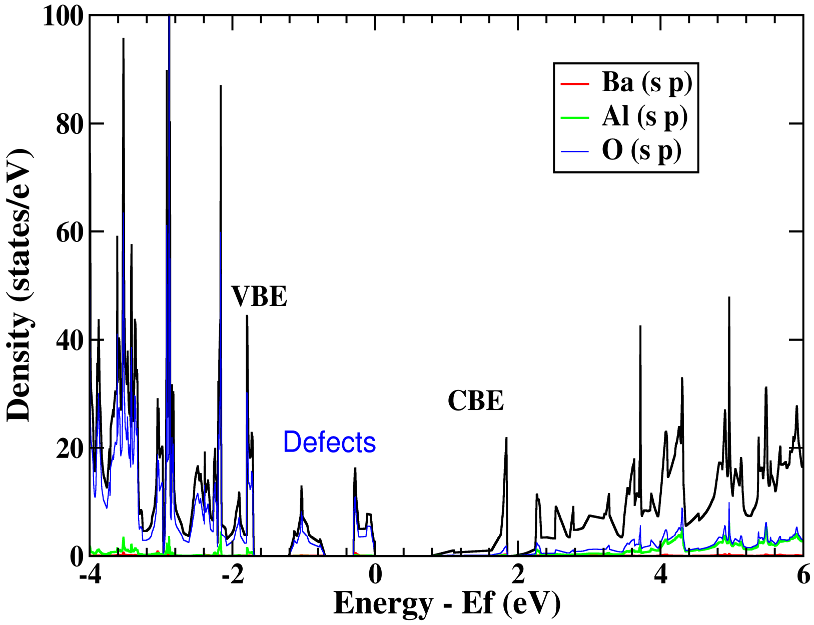

Figure 2: DOS plot around the Fermi energy (E_f, fitted at midgap) for defective BAHO structure, showing band edges (VBE and CBE) and oxygen-derived gap states.

Therefore, for simplification of defect analysis we used a perfect crystallographic cell. None such exists in the International Crystal Structure Database for BAHO, however such data does exist for CAHO.[5] As the only difference between the BAHO and CAHO systems are Ba^{2+}/Ca^{3+} ions, we simply used the same crystal for both systems. Equilibrium lattice vectors were obtained by generating energy-volume data from a series of constant volume cell shape optimisation calculations, and fitting this data to the Murnaghan equation of state. For the BAHO system we obtained $a = b = 5.641$ Å and $c = 22.461$ Å, while for the CAHO system we obtained $a = b = 5.612$ Å and $c = 22.165$ Å. Comparison with experiment demonstrates that we overestimate lattice parameters a and b by 0.3% for BAHO, and 0.9% for CAHO, while lattice parameter c is underestimated by 0.7% for BAHO and overestimated by 1.2 % for c.[5] Our structures are in good agreement with experiment. The slight underestimate along the c-axis for BAHO is a reflection of the experimental defect disorder prevalent in experimental systems. This may act to increase the lattice constant along the c-axis. Furthermore, we note that in both materials AlO_4 tetrahedra and AiO_6 octahedra coexist, while Ba/Ca reside in larger tetradecagons. The structure is shown in Figure 3.

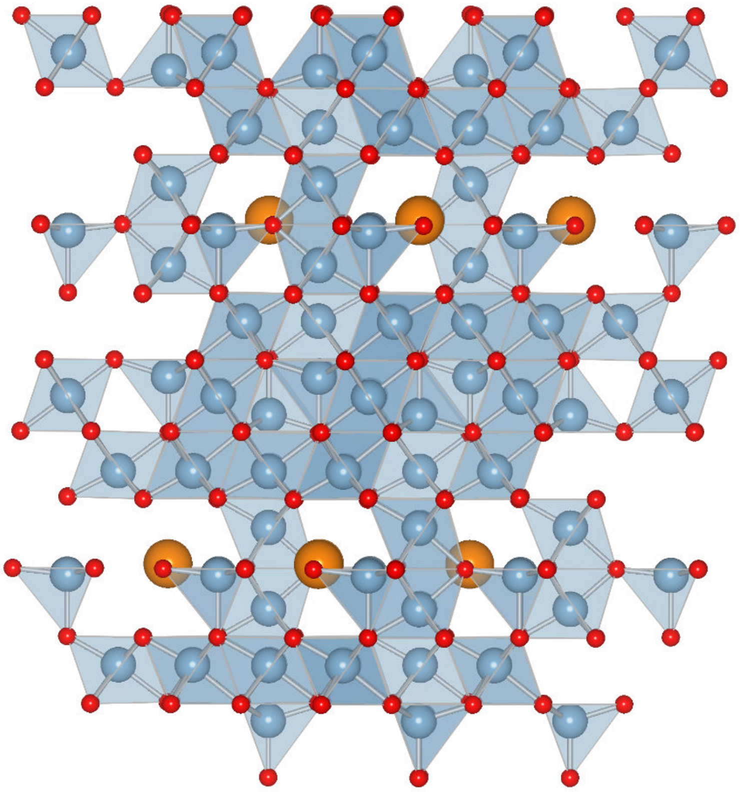

Figure 3: Crystal structure of CAHO compound, with Al atoms indicated by blue spheres, O atoms by red spheres, and Ca atoms indicated by orange spheres. Al-O bonding network are indicated by polyhedra. Significant spaces around the Ca atoms are indicated by pores. BAHO crystal structure is very similar.

An important determining factor in the thermal stability of materials is the size of the bandgap, the larger the gap the greater the stability. This is especially important for our barrier materials, which must maintain a high stability in order to prevent Fe diffusion into the alumina substrate. The DOS's of the materials are shown in Figure 4. From the DOS plot we see that both materials have a large bandgap. Indeed, with gaps approximately 4.5 eV, these are significantly greater than that of bulk haematite Fe_2O_3, suggesting both materials have a greater thermal stability than haematite, which has a bandgap of 2.2 eV. This is suggestive that haematite is stable on this material. Furthermore, CAHO has a very slightly smaller bandgap than BAHO, implying a lesser thermal stability. The similarity in electronic structures is further reflected from a calculation of the electronic contribution to the thermal conductivity, as calculated using Boltzmann Transport Theory.[6] As can be seen in Figure 5, these thermal conductivities are very similar.

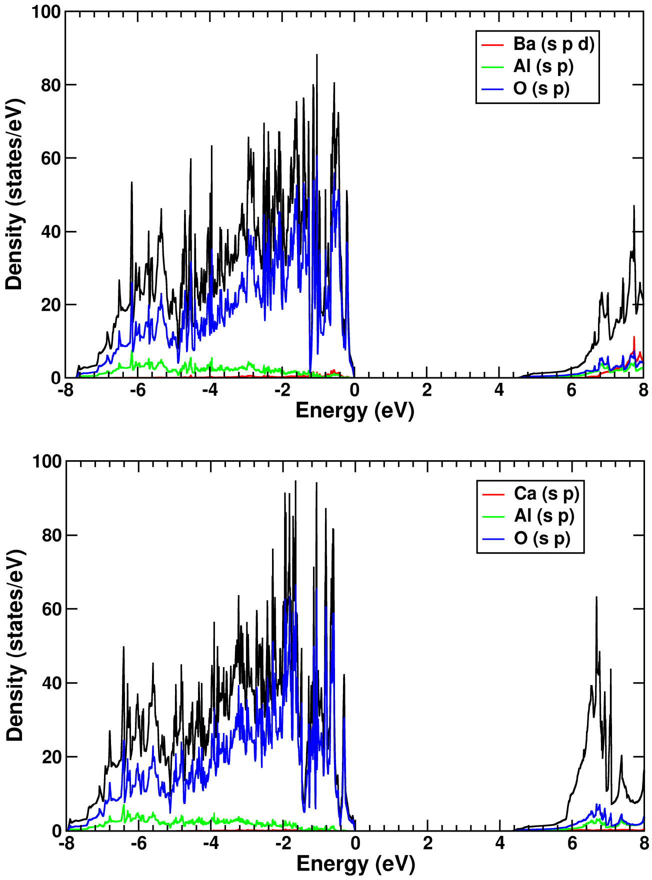

Figure 4: DOS of BAHO (top) and CAHO (bottom). The zero of the x-axis is set to the top of the valence band.

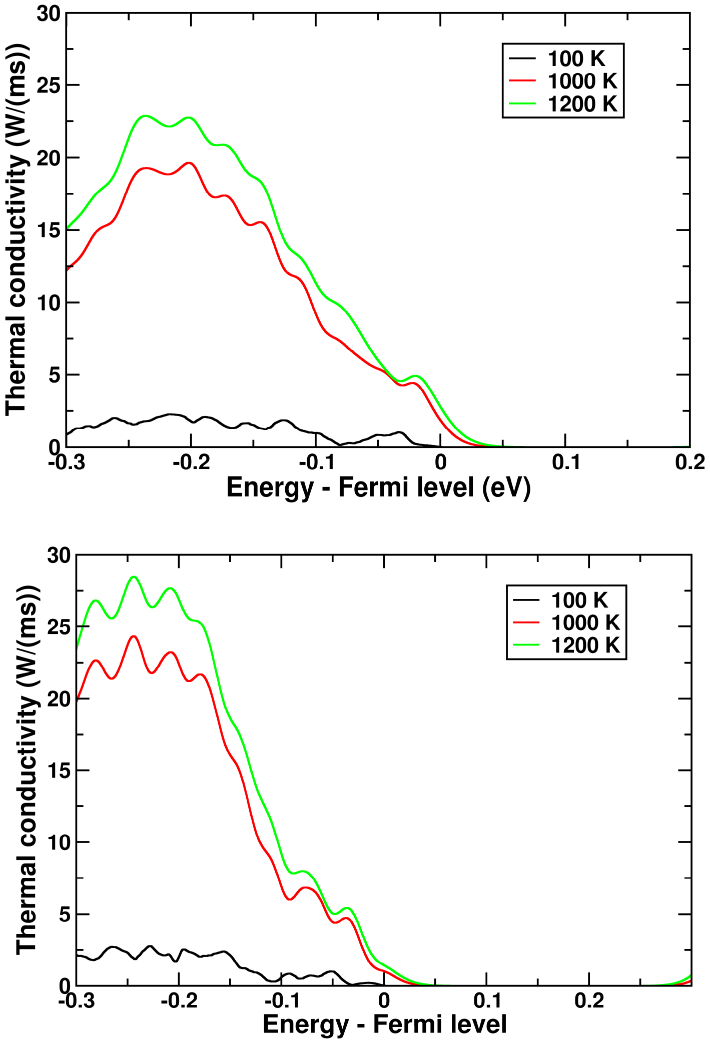

Figure 5: Electronic thermal conductivity for BAHO (top) and CAHO (bottom) materials, for three different temperatures, 100, 1000, and 1200 K.

Thermal stability determination from bandgap size are empirical in nature and only approximately accurate. This is especially the case for these systems, where we used the PBE exchange correlation functional for electronic structure analysis. This is known to severely underestimate the bandgap. Therefore, we have explicitly calculated the Helmholtz free energy of elemental decomposition of both materials, with respect to bulk aluminium, molecular oxygen, and barium or calcium. The free energy of the O_2 molecules includes pressure and temperature effects from rotation and translation of molecules. Our results as a function of temperature are shown in Figure 6. The negative free energy demonstrates that these materials are stable at low temperature. Furthermore, we find that the CAHO structure is actually more stable with respect to decomposition than the BAHO structure, with complete decomposition occurring at ~4150 K for BAHO and ~4350 K for CAHO. Based on this more detailed result, CAHO would be the superior barrier material.

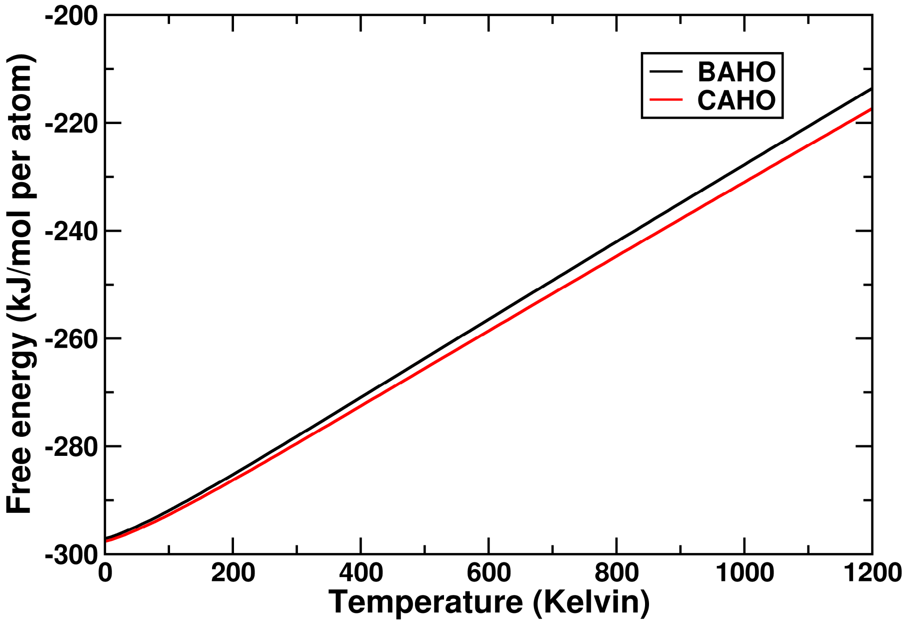

Figure 6: Helmholtz free energy for both barrier materials as a function of temperature.

As the support material will be designed to interface with the metal oxides at elevated temperature, the volume expansion coefficients are important. We can compare these to Fe_2O_3 to determine if there are significant differences. These are obtained from free energy calculations at different volumes, Figure 7. Volume expansion from 0 to 1000 K are very similar for all three materials, with BAHO having a volume change of 3.2% at 900 K, CAHO having a volume expansion of 3.0% AT 900 K, and Fe_2O_3 having a volume expansion of 2.9% at 1000 K. There will be no thermally induced support/metal oxide delamination at the operating temperature of the chemical reforming, which is vitally important in order to maintain bonding during operating conditions. However, CAHO, having a thermal expansion coefficient closer to Fe_2O_3, is the better material for supporting Fe_2O_3, and would be the superior choice.

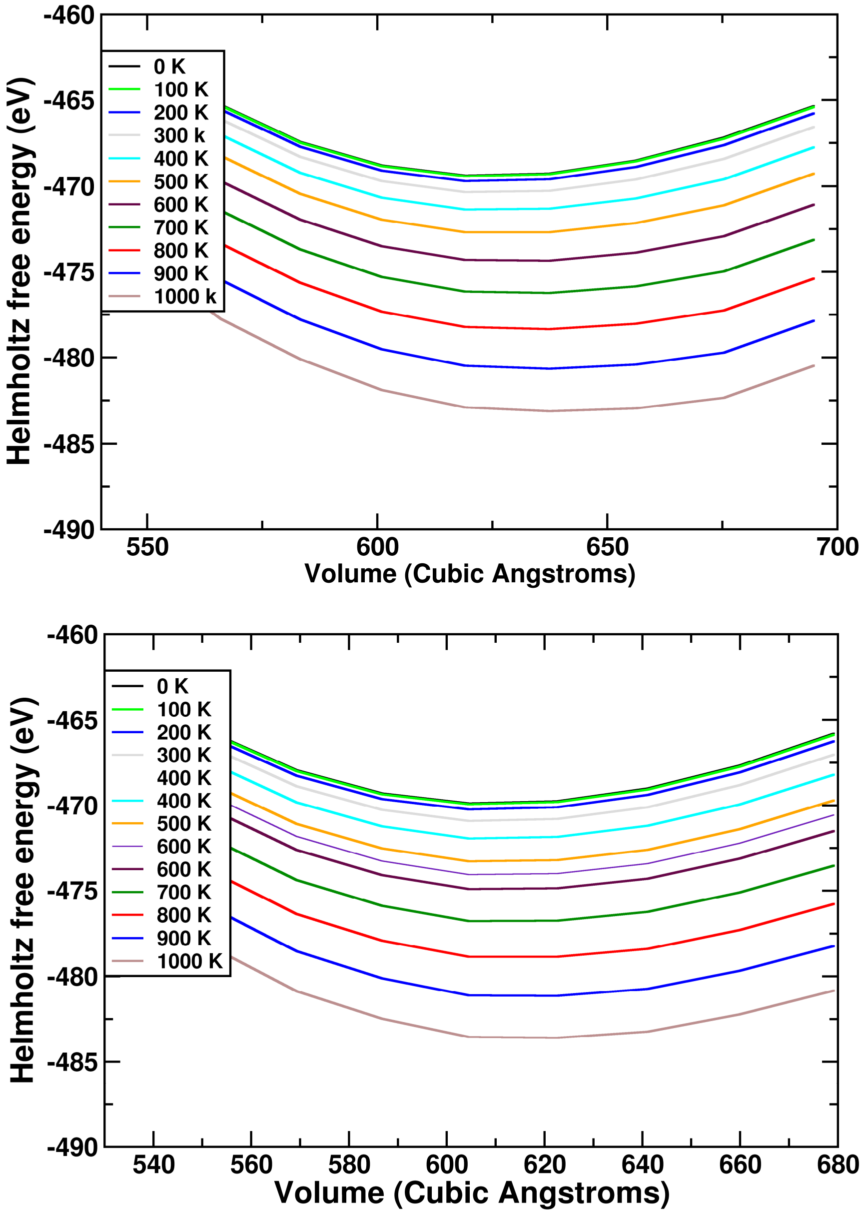

Figure 7: Helmholtz free energy plotted as function of volume for various temperatures for BAHO (top) and CAHO (bottom).

The barrier materials have to a high resistance towards either Fe incorporation into the material from haematite, or Al leaching out of the material into the haematite. In both cases, this would be deleterious to the Oxygen Carrying material as this would degrade performance. A good measurement of the ability of the material to accept Fe or leach Al is to calculate the defect formation energy, as obtained using

$$E_{form}(\alpha) = \Delta E(\alpha) + \sum_i n_i \mu_i$$

where $\Delta E(\alpha)$ is the energy difference between the defect supercell and the undefected supercell, $\boldsymbol{\mu_i}$ is the chemical potential of elemental constituent *i*, of which there are *n* types. In practice, we use the total energy of the bulk phases of the respective element as the chemical potential, e.g. bulk Fe for Fe atoms, and bulk Al for Al atoms.

We first of all consider Fe doping into the hexaaluminates. We considered three possible sites for Fe insertion into the matrix, onto one of the two possible Al sites, the Ba/Ca site or as an interstitial. The lowest energy site was the tetrahedral Al site (Fe_{Al}), see Figure 8, where Fe is in a High Spin state with a magnetic moment of 5 Bohr magnetons, with insertion into the octahedral Al site being approximately 58.0 kJ/mol higher in energy. The formation enthalpies are high, with Fe_{Al} 420.3 kJ/mol for the barium material, and 607.5 kJ/mol for the calcium material. The high formation enthalpies are due to the close packed nature of the crystal cell. This is further reflected by the larger formation energy for the Fe interstitial (Fe_I) in both crystals, at 670 kJ/mol and 850 kJ/mol for BAHO and CAHO respectively. Importantly, the calcium material is more stable towards iron incorporation due to the smaller volume of the cell, and is therefore likely the more stable material. From this analysis we would expect CAHO to be the better barrier material as it is less likely to be able to take up Fe atoms.

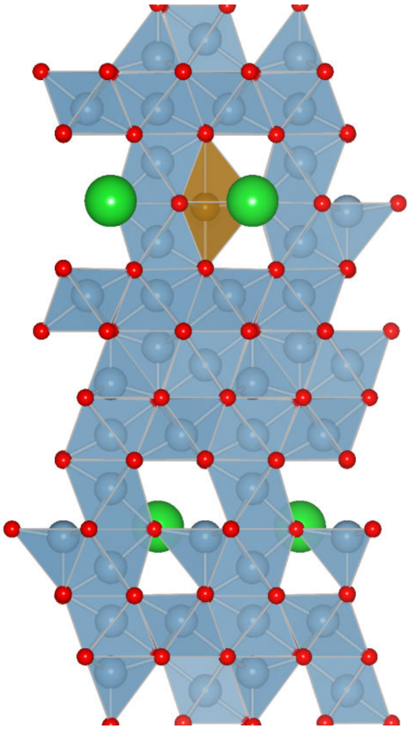

Figure 8: Crystal structure of Fe-doped CAHO structure, where Fe substitution on the tetrahedral Al atom is represented by the brown polyhedra.

We have discussed Fe insertion into the hexaaluminate matrix, however at high temperatures there is also the possibility that Al can leach from the hexaaluminate into the OC material. In order to determine if this is the case we calculated the formation enthalpy for Al vacancy formation. Based on our analysis in the previous, we analysed the CAHO structure. In this work, we are assuming that the initial crystal support is perfect and undefected, in real experimental systems this is likely to be not the case and therefore our calculations of defect formation energy are likely to be an upper limit. The lowest energy site for Al vacancy formation is the tetrahedral site, with a zero temperature defect formation energy of 1031.2 kJ/mol. An estimate of the defect formation energy can be made by assuming that the difference in free energies between the perfect and defective cells of $CaO\bullet(Al_2O_3)_6$ is proportional to the difference in stoichiometry, as we are using 252 atom supercells with lattice parameters a = b = 11.22 Å, and c = 22.17 Å, this equates to a difference of 0.4%. The assumption here is that the Al-vacancy does not strongly modify the bonds of the surrounding crystal structure. The bulk aluminium free energy is calculated as per standard means. This estimated free energy is shown in Figure 9. As can be seen, there is not a strong dependence on temperature, with the formation energy for Al removal being strongly endothermic over the entire temperature range. It is more likely that Fe will leach into the hexaaluminate matrix than Al will leach out into haematite Fe_2O_3.

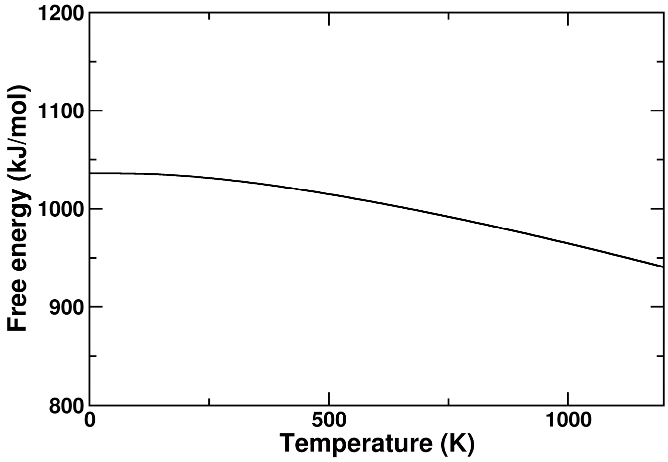

Figure 9: Helmholtz free energy of Al-vacancy formation in $CaO\bullet(Al_2O_3)_6$ as a function of temperature.

Lanthanum silicate

Late in the process, WP7 proposed a new barrier material for study in the process, lanthanum silicate in the apatite structure. It was suggested that this would be a better material as, not containing aluminium, this would be less amenable to Fe leaching via cation exchange with Al, as this material does not contain Al. To investigate, we performed calculations on the ability of the apatite material to leach Fe, and to determine the mobility of Fe through the barrier lattice.

Lanthanum silicate, hereby denoted as LASO, crystallizes in the apatite crystal structure, see Figure 10. The experimental lattice parameters are $a = b = 9.55$ Å and $c = 7.14$ Å.[7] We performed DFT-PBE calculations, with a plane wave cutoff of 520 eV. Only the gamma point in the reciprocal zone was sampled. From a fitting of the energy-volume data to the Murnaghan equation of state we found lattice parameters $a = b = 9.61$ Å and $c = 7.16$ Å, overestimates of 0.6% and 0.3% respectively for the unit cell. In the experimental samples there are ten La sites, however for charge neutrality to be maintained the ideal stoichiometry is $La_{9.333}(SiO_4)_6O_2$. There will be lanthanum site disorder. In order to accommodate a La vacancy, we use a (1×1×2) supercell, with one La atom missing, resulting in a stoichiometry of $La_{9.5}(SiO_4)O_2$. Larger supercells, with La vacancy stoichiometry closer to experiment, would be computationally more expensive and thus take a longer time to run. The PBE functional was used for all calculations.

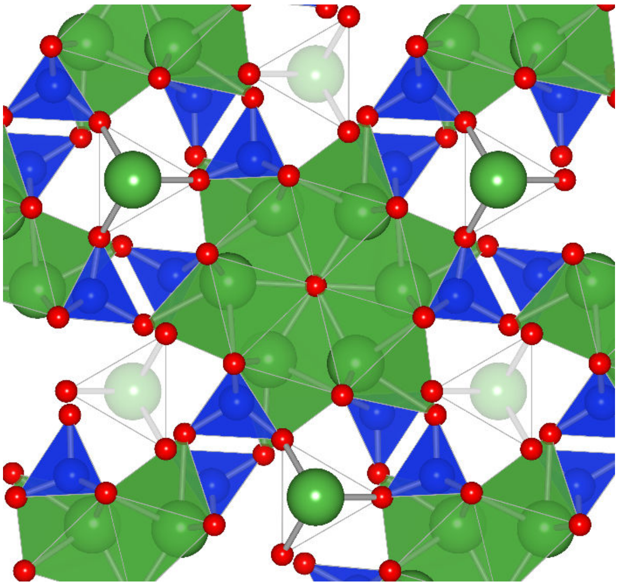

Figure 10: Crystal structure of ideal lanthanum silicate lattice. La is represented by green spheres, Si by blue spheres, and O by red spheres.

We first of all determined the energetics for Fe insertion into the lanthanum silicate lattice. We assume that Fe^{3+} will want to substitute into the La^{3+} site in order to maintain charge neutrality of the lattice. Based on the crystal structure, there are four different potential doping sites for Fe_{La} dopants. The perfect crystal has fivefold and sixfold coordinated La sites. Furthermore, as there is a La site vacancy disorder, the fivefold and sixfold coordinated sites may be near or far from the vacancy. Fe^{3+} substitution onto the vacancy site is ruled out as this would break charge neutrality, as outlined above, and thus would be significantly energetically penalized. The lowest energy Fe dopant position is the sixfold La site far from the vacancy, with a formation energy of 418.4 kJ/mol, with other dopant positions having formation energies up to 475.8 kJ/mol. Furthermore, the interstitial formation energy is higher than the Fe substitutional formation energy, at 436.2 kJ/mol.

At first glance, the lower formation energies for Fe doping into the LAOS lattice suggests that the hexaaluminate materials are better as supports than the lanthanum silicate. However, in both cases this dopant formation energy is significantly endothermic. Unlike the comparison with the hexaaluminates, the LAOS material has a significantly different crystal structure. Therefore, Fe atom transport processes for the two materials would be expected to be different, with implications for their utility as barrier materials. To this end, DFT molecular dynamics calculations at a temperature of 1400 K were performed for 30 ps duration in order to determine diffusion constants for Fe transport. The higher temperature was used as *ab initio* MD calculations are quite slow, a slightly higher temperature will accelerate diffusion, resulting in the simulation requiring less time to run in order to observe key transport properties. As for both systems interstitial Fe is the less stable, i.e. more mobile, dopant we investigated transport for this system. Diffusion constants (D_C) were calculated using the Einstein expression:

$$D_c = \frac{\Delta r^2}{2D\Delta t}$$

where Δr^2 is the total distance travelled by the end of the simulation, D is a variable related to the dimensionality of diffusion, which from observation is sheet-like, and Δt is the time elapsed in the simulation. A direct calculation of the diffusion constants finds that D_c is 4.125×10^{-6} cm^2/s for LAOS, and 6.312×10^{-6} cm^2/s for CAHO. The silicate system has a lower diffusion constant, suggesting that it is a better barrier material for resisting Fe incorporation. Furthermore, from direct observation of the atomistic processes, we see that there is one Fe transport event occurring in the MD run of the CAHO structure, wherein the Fe_I atom hops to a neighboring Fe_i site, at approximately 18 ps into the MD run, see Figure 11. No similar process occurs in the LAOS crystal over the 30 ps duration of the MD run, our calculated diffusion constant represent a maximum value for this material. Furthermore, as the LAOS crystal is significantly less dense than the CAHO crystal, at 11.3 $Å^3$/atom compared to 6.9 $Å^3$/atom, the diffusion constant we calculate is almost certainly related to Fe interstitial rattling around the lattice. Based on this analysis, we expect the LAOS material to have significantly slower and better Fe transport properties than the CAHO material. From this perspective, it will be the better barrier material.

Conclusions

We have performed DFT calculations to ascertain the suitability of different materials to act as barriers separating the active Fe-based oxygen from the Al_2O_3 support. We have compared three materials, barium and calcium hexaaluminate, and lanthanum silicate. We found that all materials have endothermic Fe dopant formation energies, with the calcium hexaluminate having the largest formation energy. Furthermore, we compared the Fe transport dynamics for the best hexaaluminate and the silicate. We found that the aluminate has poorer Fe barrier transport characteristics, i.e. that the Fe diffusion constant is larger. From our analysis, we would suggest that the lanthanum silicate is the best material. However, we caution that we assume that perfect materials have being synthesized. In real systems, grain boundaries, vacancy disorder nonstoichiometry may all be present in the synthesis. Our models are idealisations of the real systems, and consequently do not contain these factors. Final verification will need to be made by experiment.

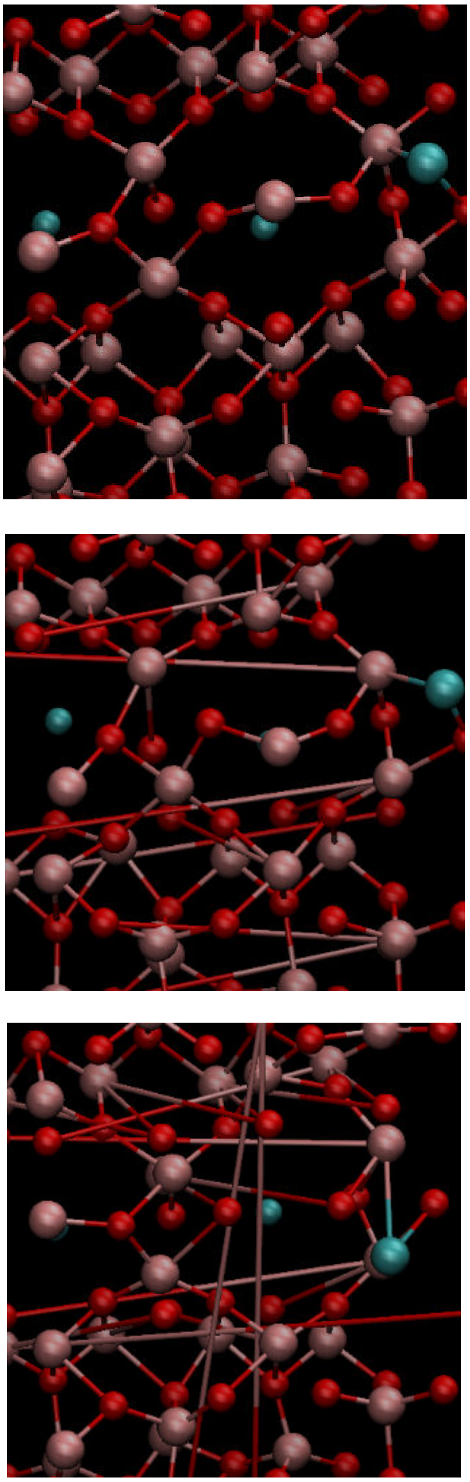

Figure 11: Initial (t = 0ps, top), at transition (t = 18 ps middle), and after transition (t= 30 ps, bottom) snapshots of Fe interstitial transport in the CAHO crystal. Fe is represented by large blue sphere, Ca by small blue sphere, Al by light pink sphere, and O by red sphere.

---

[1] Kresse, G.; Furthmuller, J., Efficiency of ab-initio total energy calculations for metals and semiconductors using a plane-wave basis set. *Computational Materials Science* **1996,** *6* (1), 15-50.

[3] Dudarev, S. L., Botton, G. A., Savrasov, S. Y., Humphreys, C. J. & Sutton, A. P. Electron-energy-loss spectra and the structural stability of nickel oxide: An LSDA+U study. *Physical Review B* **1998**, *57*, 1505-1509

[4] Rohrbach, A., J. Hafner, J., and Kresse, G. *Ab initio* study of the (0001) surfaces of hematite and chromia: Influence of strong electronic correlations *Physical Review B*, 2004, **70**, 125426.

[5] Utsonimaya, A., Tanaka, K., Morikawa, H., and Maruma, F., Structure refinement of $CaO \bullet 6Al_2O_3$, *J. Sol. Stat. Chem.* **1988**, *75*, 197-200

[6] Madsen, G. K. H. and Singh, D. J., BoltzTraP. A code for calculating band-structure dependent quantities. *Comp. Phys. Comm.* **2006**, *175*, 67-71

[7] Kuz'min, E. A., Belov, A. N. V., Crystal structure of the simplest silicates of La and Sm Doklady Akademii Nauk SSSR **1965**, *165*, 88-90